JOURNAL OF THEORETICAL AND APPLIED MECHANICS
61, 3, pp. 585-597, Warsaw 2023
https://doi.org/10.15632/jtam-pl/166466

SENSITIVITY TO GAUSS QUADRATURE OF ISOGEOMETRIC BOUNDARY ELEMENT METHOD FOR 2D POTENTIAL PROBLEMS

Ahlem Alia

Université de Lille, Centre National de la Recherche Scientifique, Centrale Lille,

Unité Mixte de Recherche 9013-LaMcube-Laboratoire de Mécanique, Multiphysique, Multiéchelle, Lille, France

e-mail: ahlem.alia@univ-lille.fr

Hasna Ben Said

Faculté des Sciences de Gafsa, Département des Filières Technologiques, Tunisia

IsoGeometric Analysis (IGA) is widely used because it links exact geometry to analysis. When IGA is applied within the Boundary Element framework (IGBEM), and under certain boundary conditions, discretization errors can be suppressed leading to an accurate estimation of the integration errors. By using the IGBEM for potential problems, the effect of Gauss quadrature on the accuracy of each term arising in the IGBEM is studied for smooth geometry under constant boundary conditions. The results show that the method of computing singular integrals in the IGBEM is efficient. Results can be improved by selecting optimal numbers of Gauss points for both integrals.

Keywords: potential problems, isogeometric analysis, boundary element method, Gauss quadrature

1. Introduction

In recent years, there has been an increasing interest in applying IsoGeometric Analysis (IGA) for mechanical problems such as solid mechanics (Chasapi *et al.*, 2022; Peng and Lian, 2022), fluid mechanics (Opstal *et al.*, 2015; Yan *et al.*, 2019), acoustics (Coox *et al.*, 2017; Alia, 2020; Alia *et al.*, 2022) and contact (Temizer *et al.*, 2011; Matzen *et al.*, 2013; Khanyile *et al.*, 2022). IGA has shown a superior precision over the conventional Finite Element Method (FEM) and Boundary Element Method (BEM) for many applications (Hughes *et al.*, 2005, 2010; Simpson *et al.*, 2012; An *et al.*, 2018). Contrary to these standard methods, IGA is based on the exact geometry because it links between the geometry design and mechanical analysis environments.

Due to Hughes (Hughes *et al.*, 2005), this numerical method uses NURBS basis functions of geometry to approximate unknowns. Since that pioneer work, other basis functions like Bsplines and Bézier have been used, and other specific algorithms have been developed for IGA. In fact, to discretize a problem, IGA is based on a patch, knot vector, control points and control variables entities. The control entities are not physical but only fictive entities. They are used to interpolate physical nodes and variables by using NURBS, Bsplines or Bézier functions. This is why, for instance, a new contact algorithm knot-to-surface has been specifically developed for IGA (Temizer *et al.*, 2011).

Studies on the accuracy of the standard BEM focused on some specific aspects such as the commonly applied rule of six elements per wavelength in acoustics for continuous elements (Marburg, 2002) and the position of collocation points on discontinuous elements (Marburg and Nolte, 2008). For 2D acoustic applications, Treeby and Pan (2009) have presented an interesting classification of BEM errors into three categories. The first category of errors originates from

discretization that is due to approximation of boundary variables, geometry, and their discontinuities. The second category of errors concerns quadrature ones because of the approximate evaluation of regular, singular and nearly singular integrals. Finally, the last category of errors is related to system resolution which exhibits ill-conditioned matrices at some irregular frequencies as well as additional errors due to the iterative solver. These three categories of errors are related to each other, so it is difficult to separate them. This is why Treeby and Pan (2009) proposed to set a global error constraint supposed to be appropriate within the engineering applications. Then they discussed precision of the method when that global error was maintained.

Some numerical aspects related to errors in IGA were analyzed in previous works (Simpson *et al.*, 2012; An *et al.*, 2018; Kostas *et al.*, 2017) including development of new quadrature formulae (Aimi *et al.*, 2018; Calabrò *et al.*, 2018) and the effect of Gauss quadrature on the accuracy of singular integrals (Peng and Lian, 2022). In fact, even if the geometry is exact, a small number of Gauss points can lead to wrong results as shown in (Alia, 2020) because the Gauss points play the role of acoustic source points. To our knowledge, there was no direct interest in estimating integration errors of different terms occurring in the boundary integral equation of potential problems when solved by the IsoGeometric Boundary Element Method (IGBEM) in the case of a standard Gauss quadrature.

The objective of this study is to identify the effect of the number of Gauss points on the accuracy of integral involving Green's function and the derivative of Green's function, separately. In fact, since in IGA simulation is performed on the exact geometry instead of the approximated one, we suppress the discretization errors by choosing constant boundary variables on a smooth geometry. In this article, before exploring in details the motioned numerical method (Section 3), we review the conventional BEM in Section 2. Finally, we validate the IGBEM results in Section 4 for an annular region before studying the influence of Gauss quadrature on the accuracy of integrals in the case of a circular domain.

2. Boundary element method for potential problems

Both the Laplace equation and the Green function are fundamental for the boundary integral formulation of potential problems (Katsikadelis, 2016). Laplace equation (2.1) governs the potential field ϕ in many problems like steady state heat conduction and potential flow inside a domain V limited by a boundary S (Liu, 2009)

$$\Delta\phi = 0 \quad \text{in} \quad V \tag{2.1}$$

The Dirichlet and Neumann boundary conditions are given, respectively, by

$$\phi = \phi_D \quad \text{on} \quad S_D \qquad\qquad q = \frac{\partial\phi}{\partial n} = q_N \quad \text{on} \quad S_N \tag{2.2}$$

where $S = S_D \cup S_N$, n is the boundary normal pointing away the domain, and q is the normal derivative of ϕ.

By using the second Green identity, the well-known Boundary Integral Equation (BIE) can be derived from the preceding boundary value problem and expressed as in the following (Liu, 2009; Wu, 2000)

$$\int_S \Big(G(P,Q)\frac{\partial\phi(P)}{\partial n} - \phi(P)\frac{\partial G(P,Q)}{\partial n} \Big)\, dS(P) = C_Q\phi(Q)$$

$$C_Q = \begin{cases} 1 & Q \in V \\ \dfrac{1}{2} & Q \in S_{smooth} \\ 0 & Q \notin (S \cup V) \end{cases} \tag{2.3}$$

Green's function is expressed in two dimensions as $G(P,Q) = -(1/2\pi)\log r$ (Liu, 2009). Here r is the distance between two points Q and P. The BIE is to be used with the Neumann condition (describing $\partial\phi_N(P)/\partial n$ on S_N) and Dirichlet condition (describing $\phi_D(P)$ on S_D).

To solve numerically the BIE for unknown boundary variables, the geometry is discretized into *ne* elements and *nd* nodes. In the case of isoparametric boundary elements, both geometry and boundary variables are represented by the same Lagrange shape functions N_i. Over an element, a varying quantity f is approximated by $f = \sum_{i=1}^{\ell} f_i N_i(u)$ where u is the local coordinate ($-1 \leqslant u \leqslant 1$) and ℓ is the number of nodes per Lagrange element. f can be the potential, derivative of the potential, or node position given by x and y. The discretized form of the BIE can be written as

$$\Big(\sum_{e=1}^{ne}\sum_{i=1}^{\ell}\int_{-1}^{\ell} G(P,Q)N_i J_e\, d\xi\Big)q_i + \Big(\sum_{e=1}^{ne}\sum_{i=1}^{\ell}\int_{-1}^{1}\frac{\partial G(P,Q)}{\partial n}N_i J_e\, d\xi\Big)\phi_i = C_Q\phi(Q) \tag{2.4}$$

where J_e is the Jacobian of transformation of the e-th element.

Despite the introduction of these boundary conditions, only half of the boundary values are known from the boundary conditions (Wu, 2000). The other half needs to be calculated by collocating the point Q on the entire boundary. Collocation consists in placing the point Q successively in each node i of the boundary. For each collocation node i and element S_j, the boundary integration based on Eq. (2.4) is performed to produce two elementary vectors in 2D problems denoted by g_i and h_i. After assembling the elementary vectors into global matrices and then arranging them in such a way that all the unknowns are located on the left-hand side, solving the obtained system enables one to calculate the boundary unknowns (Wu, 2000).

Usually, the used geometry introduces errors because it is not exact. In what follows, the exact geometry based on NURBS (Non-Uniform Rational BSplines) combined to BEM is adopted to suppress the errors due to domain approximation. The next Section concerns the definition of the NURBS basis functions and their introduction into the BEM.

3. Isogeometric boundary element method

3.1. Preliminary notions

Among the curves designed by control points, Bsplines and NURBS can be cited. It is known that Bsplines are very flexible in geometry design. Their flexibility is originating from their basis functions $N_{i,p}$ which have quasi-local control. These basis functions are different from the shape functions N_i of the standard BEM. Note the order of interpolation p in $N_{i,p}$. The basis functions $N_{i,p}$ are constructed for a knot vector, $\mathbf{E} = \{u_1, u_2, \ldots, u_{n+p+1}\}$, a non-decreasing sequence of coordinates in the parametric space. Each knot vector corresponds to a patch of elements. The knot vector can be uniform (nodes are equally-spaced in the parametric space) or not (repeated nodes) (Hughes *et al.*, 2005). It serves to divide the parametric space into elements and to modify the shape of the curve.

Equation (3.1) defines a Bspline curve T of the order p (Hughes *et al.*, 2005)

$$T(u) = \sum_{i=1}^{m} N_{i,p}(u)P_i = \mathbf{P}^{\mathrm{T}}\mathbf{N}(u) \tag{3.1}$$

where P_i are the Bspline control points, m is the number of both basis functions and control points. The basis functions $N_{i,p}$ are calculated by the following recursive expression (Hughes *et al.*, 2005)

$$N_{i,0}(u) = \begin{cases} 1 & u_i \leqslant u \leqslant u_{i+1} \\ 0 & \text{otherwise} \end{cases}$$
$$N_{i,p}(u) = \frac{u - u_i}{u_{i+p} - u_i} N_{i,p-1}(u) + \frac{u_{i+p+1} - u}{u_{i+p+1} - u_{i+1}} N_{i+1,p-1}(u) \qquad p \geqslant 1 \tag{3.2}$$

The most important properties of the Bspline basis functions are the partition of unity, Eq. (3.3), linear independence, Eq. $(3.3)_2$, and its quasi-local support because some control points influence $p+1$ elements

$$\sum_{i=1}^{m} N_{i,p}(u) = 1$$
$$\sum_{i=1}^{m} a_i N_{i,p}(u) = 0 \iff \forall i \quad a_i = 0 \tag{3.3}$$

The rational basis functions of NURBS are defined as following

$$R_{i,p}(u) = \frac{w_i N_{i,p}(u)}{\sum_{i=1}^{m} w_i N_{i,p}(u)} = \frac{\mathbf{WN}(u)}{W(u)} \tag{3.4}$$

where w_i is the weight of the i-th basis function and $W(u)$ is the weight function. Both Bsplines and NURBS shared the same properties listed above, and the NURBS curve is deduced by

$$T(u) = \sum_{i=1}^{m} R_{i,p}(u) P_i = \mathbf{P}^{\mathrm{T}} \mathbf{R}(u) \tag{3.5}$$

Besides the flexibility of Bsplines and NURBS, they present an important feature of easy refinement without deploying a great effort. In fact, three types of refinement can be used in IGA (Hughes *et al.*, 2005). In h-refinement, the knot insertion consists in adding new knots and, therefore, new elements. Each new element is located between knots of different values. During this process, the number of control points is increased by one after each knot insertion. Consequently, the control points require to be redefined at each new insertion. Moreover, the new basis functions have to be recalculated for the new knot vector. p-refinement consists of the order elevation by increasing the multiplicity of each knot component by one. This increases the number of control points and basis functions but keeps the geometry and parameterization unchanged. The last type, called k-refinement, is a combination of both knot insertion and order elevation.

3.2. Computational aspects related to IGBEM implementation

Now it is easy to link the geometry design and the analysis based on the BEM environment. Let us consider a geometry that is defined by NURBS. For a set of control points $P_i(x_i^P, y_i^P)$, the geometry of the domain is defined by

$$x = \sum_{i=1}^{m} R_{i,p}(u) x_i^P \qquad y = \sum_{i=1}^{m} R_{i,p}(u) y_i^P \tag{3.6}$$

where x, y are the coordinates of a boundary point, u is its parametric coordinate, and m is the number of control points per element.

In IGA, the potential and its normal derivative are expressed in Eq. (3.7) by the same basis functions that are used to define the geometry

$$\phi = \sum_{i=1}^{m} R_{i,p}(u) \phi_i^P \qquad \frac{\partial \phi}{\partial n} = q = \sum_{i=1}^{m} R_{i,p}(u) q_i^P \tag{3.7}$$

Unlike the traditional BEM, ϕ_i^p and q_i^p represent the potential and its normal derivative at the control points, respectively. For each collocation point P_i and element, S_j^e correspond two elementary vectors h_i and g_i given by

$$\begin{aligned} h_i &= \int\limits_{S_j^e} \frac{\partial G}{\partial n} R_{i,p}(u)\, dS = \int\limits_{-1}^{1} \frac{\partial G}{\partial n} R_{i,p} J_e\, du \\ g_i &= \int\limits_{S_j^e} G R_{i,p}(u)\, dS = \int\limits_{-1}^{1} G R_{i,p} J_e\, du \end{aligned} \tag{3.8}$$

Since the control points do not necessary belong to the boundary, they cannot play the role of collocation points in the IGBEM. Instead, Greville abscissae are used as collocation points for the IGBEM (Kostas *et al.*, 2017; Johnson, 2005). Their expression is given by

$$u_i^{col} = \sum_{j=1}^{p} \frac{u_{i+j}}{p} \tag{3.9}$$

where u_i is the i-th component of the knot vector.

When the collocation point Q_i does not belong to the element S_j^e, the integral is regular and Gauss quadrature can be used as expressed in Eq. (3.10). In Eq. (3.10), $f_i^{(1)} = (\partial G/\partial n) R_{i,p}(u_k) J_e$ and $f_i^{(2)} = G R_{i,p}(u_k) J$ are two functions evaluated at the k-th Gauss point u_k of weight w_k. Moreover, $nGpR$ represents the number of Gauss points used in the regular integration

$$h_i = \sum_{k=1}^{nGpR} f_i^{(1)} w_k \qquad g_i = \sum_{k=1}^{nGpR} f_i^{(2)} w_k \tag{3.10}$$

To show the superiority of the IGBEM over BEM in the case of regular integrals, we consider convergence of $I_0 = \int dS/r^2$ over a quarter circle of radius 2 (Fig. 1). The calculation of the L_2 norm of the relative error is based on the analytical scheme provided by Mahajerin (1983) for 19 points denoted by P in Fig. 1.

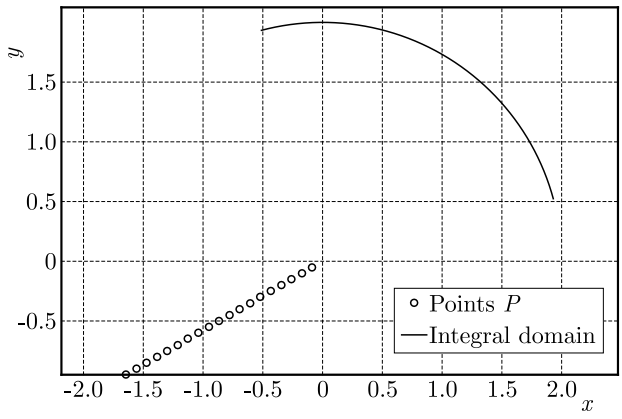

Fig. 1. Geometry of the quarter circle and location of points used to calculate integral $I_0 = \int dS/r^2$

Figure 2a represents a clear illustration of the accuracy of the IGBEM. Actually, only 4 elements and 4 Gauss points are required to integrate $1/r^2$ over the quarter circle. 4 Gauss points and 10 elements are sufficient to achieve an error of the machine precision order. With only 2 Gauss points and 10 elements, we obtain an error of the order of 10^{-8}. On the other hand, the BEM seems to be less accurate than the IGBEM. In fact, BEM errors are greater than those

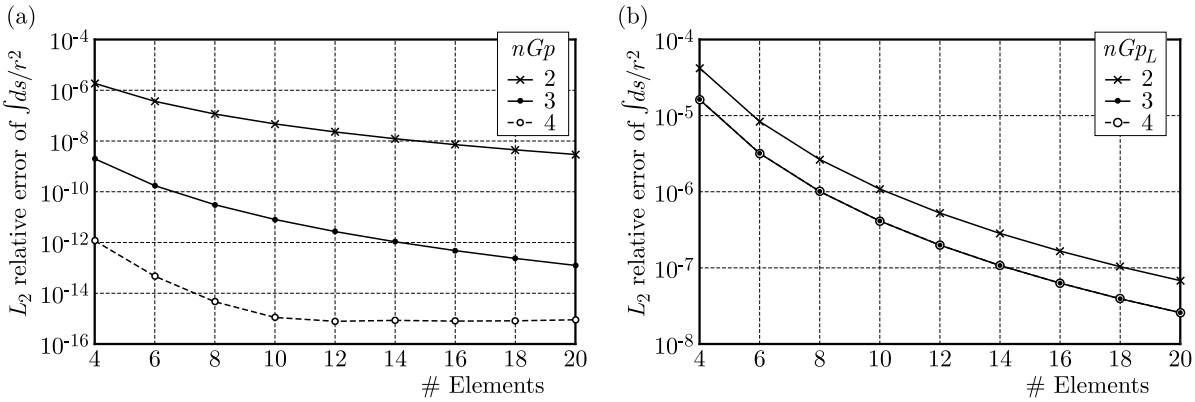

Fig. 2. Errors in the evaluation of $I_0 = \int dS/r^2$ over the quarter circle with respect to the elements number for different numbers of Gauss points in the case of (a) IGBEM and (b) BEM

of the IGBEM (Fig. 2b). In the BEM, the minimum error of the order of 10^{-7} is archived for 3 Gauss points and cannot be improved anymore by increasing the number of Gauss points.

When the collocation point Q_i belongs to the element S_j, the integral is singular. To overcome the singularity problem, the procedure proposed initially by Wu (2000) for the BEM is applied and adopted here to the IGBEM. It consists in dividing the element at the collocation point into left and right regions and improving the convergence rate by considering two successive changes of variables (1) $z^2 = \varepsilon(u_p - u)$, and (2) $z = \sqrt{1+\varepsilon u_p}(1+\eta)/2$ where u_p is the position of the collocation point in the parametric space. The integration over the left region $\varepsilon = +1$ is performed separately from the right region $\varepsilon = -1$ in Eq. (3.11). For both regions, we use the same number of Gauss points $nGpS$. These variable changes apply also to the elementary vector h_i. Therefore, Eq. (3.11) written for g_i can be extended to h_i by only replacing the Green function by its normal derivative

$$g_i^{(\varepsilon)} = \int_0^{\sqrt{1+\varepsilon u_p}} GR_{i,p} J_e 2z \, dz = \int_{-1}^{1} GR_{i,p} J_e 2z \frac{dz}{d\eta} \, d\eta \tag{3.11}$$

Finally, when the collocation point lies close to the element but not in, then the integral is nearly singular. In this paper, we choose to treat the nearly singular integrals exactly as the regular ones without any additional treatment. The consequences of this choice will be discussed later. In what follows, the number of degrees of freedom is denoted by $nDOF$ for IGBEM and $nDOF_L$ for the BEM, where L is used for Lagrange.

4. Results

The previous equations have been implemented to handle several patches and closed domains, and numerical simulation is performed only for quadratic elements. To validate the IGBEM result, we consider an annular region for which the potential field ϕ_a is prescribed on the inner boundary S_a of radius a. The outer boundary S_b of radius b is subjected to the normal derivative $\partial\phi_b/\partial n$.

The analytical solution of this axisymmetric problem is given by (Liu, 2009)

$$\phi(r) = \phi_a + b\frac{\partial \phi_b}{\partial n} \log \frac{r}{a}$$

In simulation, we used the following parameters: $a = 1$ with $\phi_a = 100$, and $b = 2$ with $\partial\phi_b/\partial n = 200$.

For a clear illustration of the IGBEM mesh, a small number of elements of the same length ($ne = 24$, $nDOF = 32$) have been used to plot Fig. 3a in the case of the IGBEM. Figure 3b shows the internal field points used to calculate the potential field inside the annular region. These internal field points are located between $r = 1.1$ and $r = 1.9$.

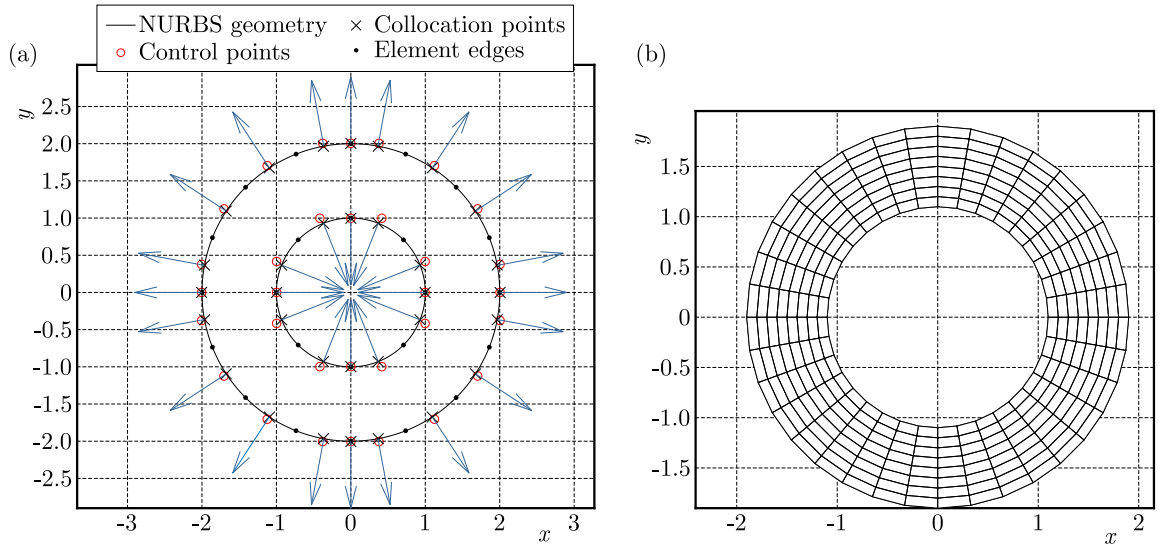

Fig. 3. (a) NURBS-based geometry and the IGBEM mesh of the annular region, (b) mesh of the internal points

Contrary to the BEM, IGBEM looks to be in good agreement with the analytical solution in terms of potential distribution inside the annular region (Fig. 4). Note that the BEM result has been obtained for the same number and type of elements, i.e. 24 quadratic elements but with $nDOF_L = 48$.

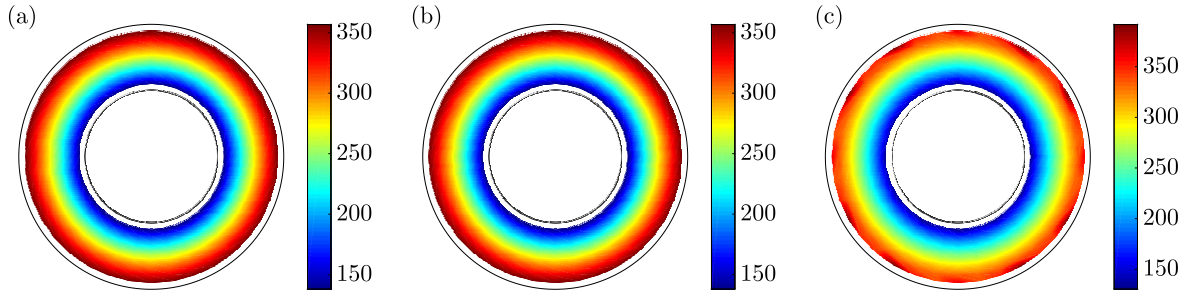

Fig. 4. (Color online) Potential distribution calculated: (a) analytically, (b) by IGBEM, (c) BEM

For a better comparison, the relative error for the field points located on x-axis is plotted in Fig. 5. One can see that the quality of the IGBEM solution is better than that of the BEM but the IGBEM appears less accurate for points close to the boundaries in comparison to points located far from the boundary. Consequently, we can conclude that: (1) nearly singular integrals are poorly integrated and (2) treatment of the singular integrals is sufficient. To check this initial conclusion, leting examine in detail the errors made separately on the integrals of the Green function and its derivative noted, respectively, by

$$I_1 = \int G(P,q)\, dS \qquad I_2 = \int \frac{\partial G}{\partial n}(P,q)\, dS$$

In what follows, instead of computing I_1 and I_2 over the annular region, the geometry is simplified. From now on, let us limit the geometry to only the outer boundary of the last example, i.e. a circle of radius 2 as shown in Fig. 6.

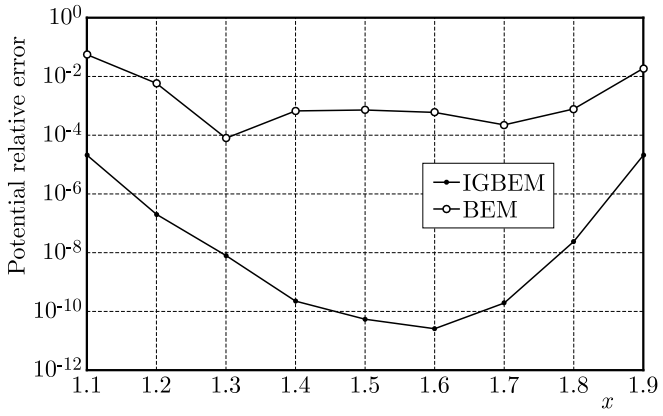

Fig. 5. Errors in the potential at internal field points located on the x-axis for IGBEM and BEM

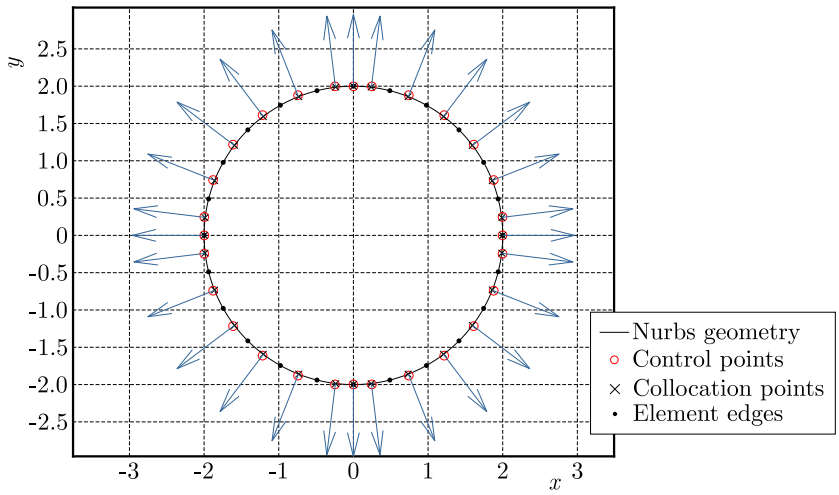

Fig. 6. NURBS-based geometry and the IGBEM mesh of the circle

4.1. Errors in $I_1 = \int [\partial G(Q,P)/\partial n]\, dS(P)$

To examine the quadrature errors, we considered the case of an internal potential problem consisting of a circle of radius 2. A simple way to study the quadrature error in the term involving the normal derivative of Green's function $I_1 = \int [\partial G(P,Q)/\partial n]\, dS(P)$ is to calculate $C_Q = -\int [\partial G(P,Q)/\partial n]\, dS(P)$. The exact value of C_Q is given by Eq. (2.3).

To show the superior precision of the IGBEM over BEM, the variation of the regular integral error of C_Q at an internal point as it gradually approaches the boundary of the circle along the x direction is plotted in Fig. 7a. Note that in this figure, x varies from -1.99 to 1.99 with a space step of 0.0025 in order to show all variations. As expected, the IGBEM behaves better than the BEM. In fact, to obtain the same error, the IGBEM requires almost a half of the number of degrees of freedom required by the BEM. When the point is far from the boundary, the regular integral error is of the order of the machine precision (Fig. 7a) but it increases as the mesh gets coarser (Fig. 7b).

For points close to the boundary, the integral is nearly singular. One way to improve the precision is to increase the number of Gauss points for all elements (Fig. 8a). The other way is to gradually increase the number of Gauss points as the point gets closer to the integration element (Fig. 8b). To limit the maximum value of error to 10^{-8} in Fig. 8b almost everywhere, 30 Gauss points have been used to the points close to the boundary (within the size of an element). According to their distance from the boundary, 8, 6, or 4 Gauss points have been considered for the other points.

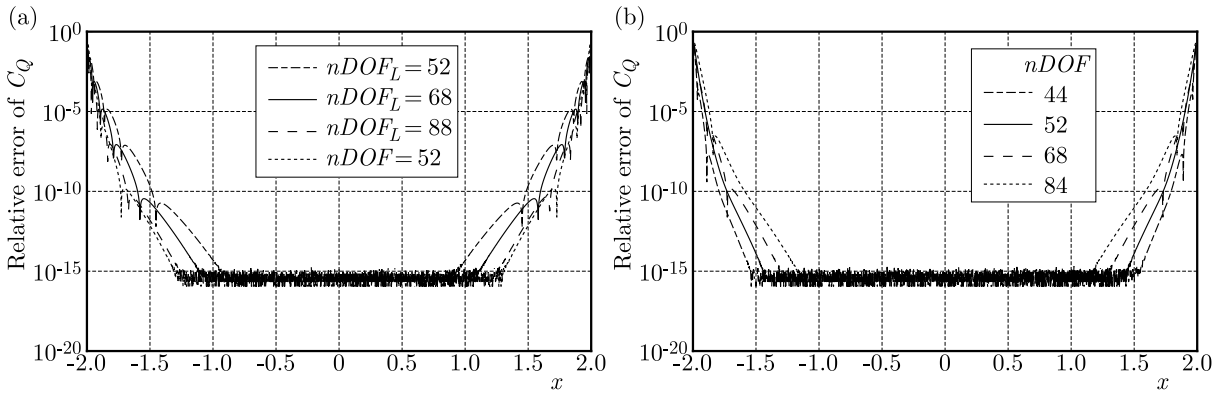

Fig. 7. Variation of errors of C_Q at an internal point as it gradually approaches the boundary of a circle: (a) comparison between the BEM and IGBEM for 6 Gauss points per quadratic element, (b) effect of DOF number for 6 Gauss points per quadratic element. $nDOF$ and $nDOF_L$ denote the DOF numbers in IGBEM and BEM, respectively

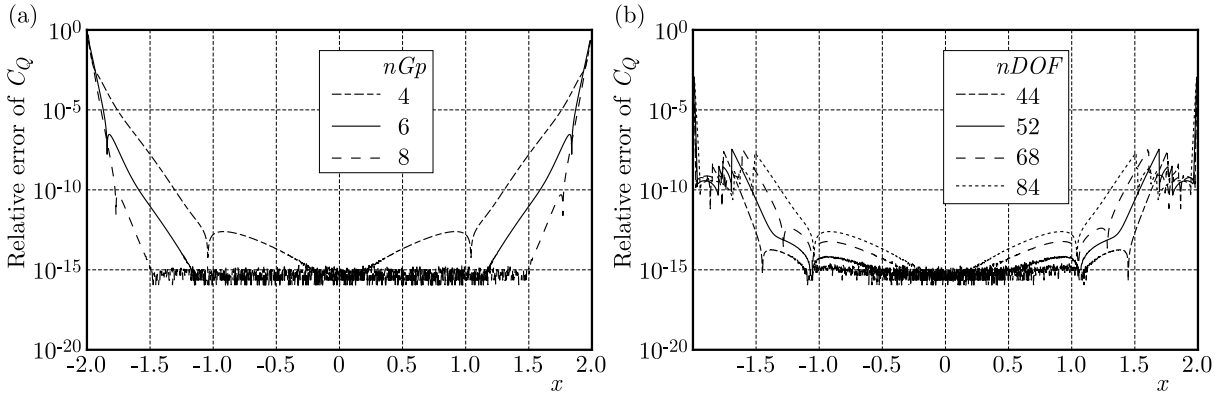

Fig. 8. Variation of errors of C_Q at an internal point as it gradually approaches the boundary of a circle: effect of (a) the number of Gauss points for 44 DOF and (b) gradual increase of the number of Gauss points as the internal point gets closer to the boundary

To our surprise, the variation of C_Q errors at collocation points presents an optimal number of Gauss points denoted by nGp^*. This optimal number increases when the mesh gets coarser as shown in Fig. 9a. For example, this optimal number is equal to 4 for 68 and 84 DOF. It is equal to 5 for 52 DOF.

To examine this result, we perform integration by using different numbers of Gauss points for singular and regular integrals that we denoted by $nGpS$ and $nGpR$, respectively, in Figs. 9b and 9c. These figures show variation of C_Q errors for 52 and 84 DOF. According to Fig. 9a, the error in the case of 84 DOF is minimal when $nGp^* = 4$. In Fig. 9b, we can see that by varying $nGpR$ from 2 to 20 in the case of 84 DOF while maintaining $nGpS = nGp^* = 4$, the error decreases in comparison to the case when $nGpS = nGpR$ and becomes constant for $nGpR \geqslant 4$. However, if $nGpR = nGp^* = 4$ then we obtain the same error as in the case of $nGpS = nGpR$ (see the case of 84 DOF in Fig. 9c). This is also true for 52 DOF.

We conclude that the overall error in I_1 is dominated by the contribution of quadrature errors of the singular integrals. The choice of the $nGpS$ number is crucial for obtaining a better precision. As soon as the optimal number nGp^* is chosen to be equal to the number of Gauss points for singular integrals, one can afford to use the lower number $nGpR$ and obtain the same quality of precision.

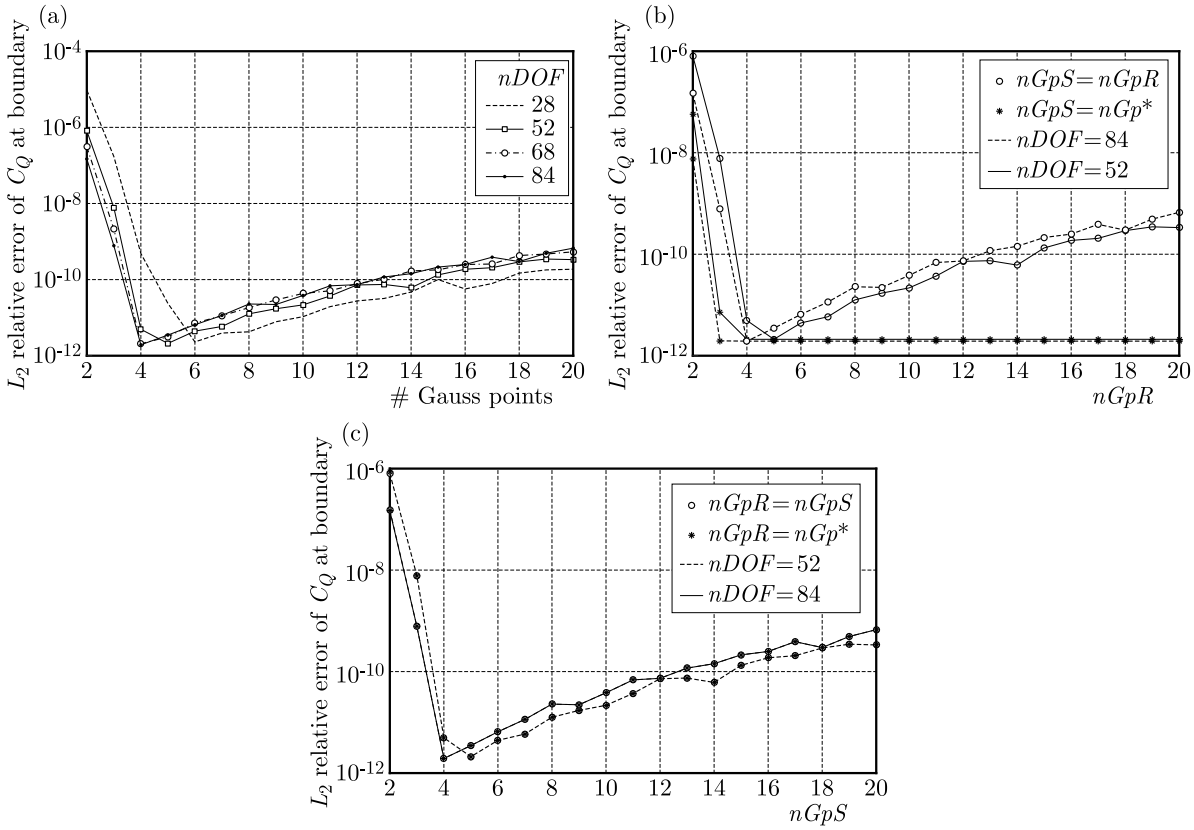

Fig. 9. Influence of the number of Gauss points on convergence of C_Q at collocation points: (a) identification of an optimal number of Gauss points nGp^* improving the convergence and effect of selection of the number of Gauss points on the precision of (b) regular integrals and (c) singular integrals for 52 and 84 DOF. $nGpS$ and $nGpR$ denote the number of Gauss points used in singular and regular integrals, respectively. nGp^* is the optimal number of Gauss points as obtained from Fig. 9a

4.2. Errors in $I_2 = \int G(Q,P)\, dS(P)$

In this Section, we study the quadrature error in the term involving Green's function denoted by $I_2 = \int G(Q,P)\, dS(P)$. The reference solution is computed using analytical integration on an arbitrary line segment proposed by Liu (2009). In Fig. 10 the variation of the regular integral error of I_2 is plotted at an internal point as it gradually approaches the boundary of the circle.

According to this figure, I_2 behaves like I_1 for internal points. Firstly, the IGBEM is more accurate than the BEM (see Figs. 7a and 10a). Secondly, when calculated with the IGBEM, the precision of I_2 can be improved by either increasing the number of Gauss points or by using fine meshes (see Figs. 10b and 10c). Another similarity with I_1 is that a better precision is achieved far from the boundary contrary to points situated near the boundary for which computing of nearly singular integrals is required. However, I_2 convergence is obtained with a higher error in comparison to I_1. Actually, by comparing Fig. 10b to Fig. 7b, we can see that for the same DOF number, the error is the highest in I_2. Moreover, the effect of the nearly singular integrals is less important in I_2 than in I_1: the range of points with the smallest error was wider in I_2 than in I_1. Therefore, far from the boundary, the regular terms in I_2 require more Gauss points than in I_1 (see Figs. 10c and 8a), but close to the boundary, I_2 behaves better than I_1.

I_2 behaves differently from I_1 when the collocation points are involved in the integral. From Fig. 11a, one can notice the absence of an optimal number of Gauss points. On the contrary, the error decreases by increasing either DOF or number of Gauss points. Moreover, I_2 convergence has a higher error than I_1 even by using 20 Gauss points in comparison, for example, to 10 in the

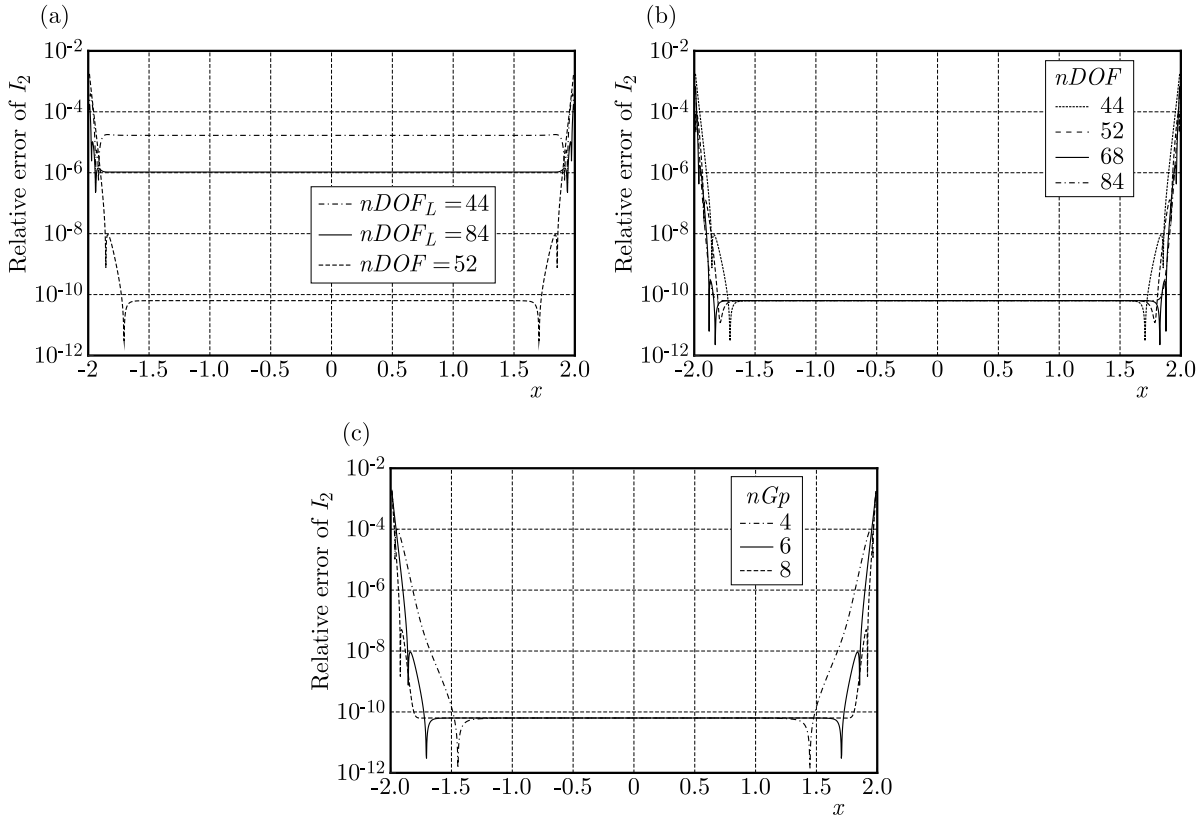

Fig. 10. Variation of I_2 errors at an internal point as it gradually approaches the boundary of a circle: (a) comparison between the BEM and IGBEM for 6 Gauss points per quadratic element, and the effect of (b) DOF number for 6 Gauss points per quadratic element and (c) the number of Gauss points for 44 DOF

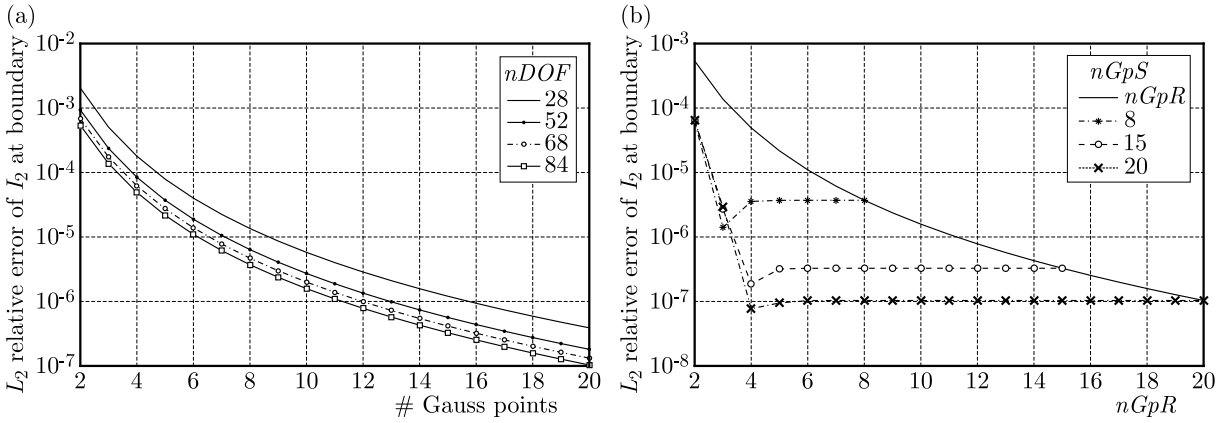

Fig. 11. Influence of the number of Gauss points on the convergence of I_2 at the collocation points: (a) for different DOF numbers and (b) effect of the number of Gauss points on errors for 84 DOF. *nGpS* and *nGpR* denote the number of Gauss points used in singular and regular integrals, respectively

case of I_1 (Fig. 9a). Since the regular integrals in I_2 give small errors, consequently, the noticed large error in Fig. 11a originates from the contribution of singular integrals. This conclusion can be confirmed by examining Fig. 11b according to which for a given *nGpS* number (for example 20) fewer nGpR Gauss points are needed (5 in our example) to obtain the same error. A more interesting result is that for a given *nGpS* number, there is an optimal *nGpR* number for which a smaller error is obtained (4 in our example).

5. Conclusion

Thanks to isogeometric analysis, the geometry is exact and its discretization errors in the IGBEM can be suppressed. This allows a better estimation of quadrature errors when constant boundary conditions are assumed over a smooth geometry. In this article, we have examined separately quadrature errors of the integral involving the derivative of Green's function (noted I_1) and that one involving Green's function itself (noted I_2) in the case of a 2D potential problem. We evaluated these integrals for points inside the domain (case of regular integrals only) and for points on the boundary (case of both regular and singular integrals).

Our important result is the identification of an optimal number of Gauss points for singular integrals of I_1. Moreover, although this number is absent in the case of singular integrals of I_2, we found that for each number of Gauss points chosen for singular integrals in I_2 there corresponds an optimal number of Gauss points for regular integrals. These results indicate that with a judicious choice of the number of Gauss points for the singular and regular integrals of I_1 and I_2 we can improve convergence of the IGBEM. Moreover, we found that I_1 is more accurate than I_2. Nevertheless, convergence remains dictated in both cases by the number of Gauss points used in the singular integrals.

In addition, the use of the Greville abscissae and the treatment of singularity by splitting the integration domain into two regions limits generalization of these conclusions. The study of the behavior of the errors for other techniques of singularity treatment and other collocation point positions deserves further investigations. Finally, our choice to compute the regular and nearly singular integrals in the same way led to large errors at points located near the boundary compared to the singular integrals. Hence, we need to give more importance to these integrals by treating them more rigorously.

References

1. Aimi A., Calabrò F., Diligenti M., Sampoli M.L., Sangalli G., Sestini A., 2018, Efficient assembly based on B-spline tailored quadrature rules for the IgA-SGBEM, *Computer Methods in Applied Mechanics and Engineering*, **331**, 327-342

2. Alia A., 2020, Ultrasonic diffraction by a circular transducer: Isogeometric analysis sensitivity to full Gauss quadrature points, *Journal of the Acoustical Society of America*, **147**, 2, EL74-EL79

3. Alia A., Khanyile N.P., Dufrénoy P., De Saxcé G., 2022, Vibration and acoustic radiation of an impacted plate: parametric study based on isogeometric analysis, *International Conference on Noise and Vibration Engineering (ISMA 2022)*

4. An Z., Yu T., Bui T.Q., Wang C., Trinh N.A., 2018, Implementation of isogeometric boundary element method for 2-D steady heat transfer analysis, *Advances in Engineering Software*, **116**, 36-49

5. Calabrò F., Falini A., Sampoli M.L., Sestini A., 2018, Efficient quadrature rules based on spline quasi-interpolation for application to IGA-BEMs, *Journal of Computational and Applied Mathematics*, **338**, 153-167

6. Chasapi M., Mester L., Simeon B., Klinkel S., 2022, Isogeometric analysis of 3D solids in boundary representation for problems in nonlinear solid mechanics and structural dynamics, *International Journal for Numerical Methods in Engineering*, **123**, 5, 1228-1252

7. Coox L., Atak O., Vandepitte D., Desmet W., 2017, An isogeometric indirect boundary element method for solving acoustic problems in open boundary domains, *Computer Methods in Applied Mechanics and Engineering*, **316**, 186-208

8. Hughes T.J.R., Cottrell J.A., Bazilevs Y., 2005, Isogeometric analysis: CAD, finite elements, NURBS, exact geometry and mesh refinement, *Computer Methods in Applied Mechanics and Engineering*, **194**, 39-41, 4135-4195

9. Hughes T.J.R., Reali A., Sangalli G., 2010, Efficient quadrature for NURBS-based isogeometric analysis, *Computer Methods in Applied Mechanics and Engineering*, **199**, 5-8, 301-313
10. Johnson R.W., 2005, Higher order B-spline collocation at the Greville abscissae, *Applied Numerical Mathematics*, **52**, 1, 63-75
11. Katsikadelis J.T., 2016, *The Boundary Element Method for Engineers and Scientists, Theory and Applications*, Academic Press
12. Khanyile N.P., Alia A., Dufrénoy P., De Saxcé G., 2022, Acoustic radiation simulation of forced vibrating plates using isogeometric analysis, *Journal of the Acoustical Society of America*, **152**, 1, 524-539
13. Kostas K.V., Ginnis A.I., Politis C.G., Kaklis P.D., 2017, Shape-optimization of 2D hydrofoils using an isogeometric BEM solver, *Computer-Aided Design*, **82**, 79-87
14. Liu Y., 2009, *Fast Multipole Boundary Element Method: Theory and Applications in Engineering*, Cambridge University Press, New York
15. Mahajerin E., 1983, Exact evaluation of $\int dSr^2$ over a circular element, *Applied Mathematical Modelling*, **7**, 4, 282-284
16. Marburg S., 2002, Six boundary elements per wavelength: is that enough? *Journal of Computational Acoustics*, **10**, 1, 25-51
17. Marburg S., Nolte B. (Editors), 2008, *Computational Acoustics of Noise Propagation in Fluids – Finite and Boundary Element Methods*, Springer, Heiderberg
18. Matzen M.E., Cichosz T., Bischoff M., 2013, A point to segment contact formulation for isogeometric, NURBS based finite elements, *Computer Methods in Applied Mechanics and Engineering*, **255**, 27-39
19. Opstal van T., Fonn E., Holdahl R., Kvamsdal T., Kvarving A.M., Mathisen K.M., Nordanger K., Okstad K.M., Rasheed A., Tabib M., 2015, Isogeometric methods for CFD and FSI-simulation of flow around turbine blades, *Energy Procedia*, **80**, 442-449
20. Peng X., Lian H., 2022, Numerical aspects of isogeometric boundary element methods: (nearly) singular quadrature, trimmed NURBS and surface crack modeling, *Computer Modeling in Engineering and Sciences*, **130**, 1, 513-542
21. Simpson R.N., Bordas S.P.A., Trevelyan J., Rabczuk T., 2012, A two-dimensional isogeometric boundary element method for elastostatic analysis, *Computer Methods in Applied Mechanics and Engineering*, **209-212**, 87-100
22. Temizer I., Wriggers P., Hughes T.J.R., 2011, Contact treatment in isogeometric analysis with NURBS, *Computer Methods in Applied Mechanics and Engineering*, **200**, 9-12, 1100-1112
23. Treeby B.E., Pan J., 2009, A practical examination of the errors arising in the direct collocation boundary element method for acoustic scattering, *Engineering Analysis with Boundary Elements*, **33**, 11, 1302-1315
24. Wu T.W., 2000, *Boundary Element Acoustics, Fundamentals and Computer Codes*, WIT Press, Southampton
25. Yan J., Lin S., Bazilevs Y., Wagner G.J., 2019, Isogeometric analysis of multi-phase flows with surface tension and with application to dynamics of rising bubbles, *Computers and Fluids*, **179**, 777-789

Manuscript received February 9, 2022; accepted for print May 9, 2023